Magnetic resonance imaging of meningiomas.

R D Zimmerman, C A Fleming, L A Saint-Louis, B C Lee, J J Manning and M D Deck

AJNR Am J Neuroradiol 1985, 6 (2) 149-157
http://www.ajnr.org/content/6/2/149

Magnetic Resonance Imaging of Meningiomas

Robert D. Zimmerman[1]
Cynthia A. Fleming
Leslie A. Saint-Louis
Benjamin C. P. Lee
John J. Manning
Michael D. F. Deck

Twenty-eight patients with 32 meningiomas were studied on a 0.5-T superconductive magnetic resonance (MR) imager. This common, benign treatable tumor was more clearly seen on computed tomography (CT) than MRI in 53% of cases. This is a result of poor contrast between the tumor and the adjacent brain on all spin-echo and inversion-recovery pulse sequences. Those sequences that provide the greatest anatomic detail were best for identifying this low-contrast lesion. Inversion-recovery scans in particular demonstrated the tumor as a discrete hypointense mass (relative to nearby white matter) with excellent visualization of the dural base and white matter buckling indicative of extracerebral mass effect. Other characteristic features include: (1) a hypointense rim because of the venous capsule (66%); (2) mottling due to hypervascularity; (3) a well defined edema collar that demarcates the tumor from adjacent brain; and (4) hyperostosis with thickening of the calvaria and obliteration of its normal landmarks. MRI did not demonstrate tumor calcification but did demonstrate vascular encasement, displacement, and occlusion better than CT and as well as digital venous angiography.

Magnetic resonance imaging (MRI) has proven to be an extraordinarily sensitive imaging method for central nervous system pathology, often exceeding computed tomography (CT) in demonstrating lesions [1–7]. Reports of MRI in meningiomas have, however, been scant and anecdotal [2, 3, 5, 6, 8]. We report our experience of MRI in 28 patients with 32 meningiomas. In this common, benign, and generally treatable lesion [9, 10], CT is more sensitive than MRI. The causes of this phenomenon will be discussed and specific MRI features of meningiomas presented.

Subjects and Methods

Twenty-eight patients were studied on a 0.5-T superconductive MR imager. All patients were studied with 8- to 13-mm-thick slices obtained by single slice, three-dimensional anisotropic, or two-dimensional Fourier transformation multislice single-echo technique. The images were routinely obtained in the axial plane and, where indicated, in sagittal and/or coronal planes. Several pulse sequences were used in each patient (average of three sequences per patient) including spin echo (SE) with an echo delay time (TE) of 30–120 msec and a repetition time (TR) of 150–2500 msec. Inversion recovery (IR) scans were performed with an inversion time (TI) of 450 msec and a repetition time (TR) of 1500 msec in 19 cases.

Each patient had a contrast-enhanced CT scan before MRI; therefore, the location and probable nature of the lesions were known before the MRI study. There were 18 female and 10 male patients aged 20–74 years (mean, 67.75). Three patients had multiple meningiomas. Seven patients with recurrent meningiomas were evaluated in this series. The lesions were distributed throughout the cranial cavity, with a preponderance of basal tumors: 10 were in the middle fossa, eight were in the anterior fossa, three were in the posterior fossa, five were in the convexity, and six were parasagittal. The sensitivities of MRI and CT were compared. The relative contrast between the tumor and the adjacent cortex was determined with all pulse sequences. Features that might confer diagnostic specificity were tabulated.

Received September 19, 1984; accepted after revision November 23, 1984.

Presented at the annual meeting of the American Society of Neuroradiology, Boston, June 1984.

[1] All authors: Department of Radiology, Division of Neuroradiology, New York Hospital–Cornell Medical Center, 525 E. 68th St., New York, NY 10021. Address reprint requests to R. D. Zimmerman.

AJNR 6:149–157, March/April 1985
0195–6108/85/0602–0149

TABLE 1: **Contrast Relative to Adjacent Cortex**

	No.	Hypointense	Minimal Hypointense	Isointense	Minimal Hyperintense	Hyperintense
SE 30/500	32	4	8	20	0	0
SE 60/1000	8	0	1	7	0	0
SE 90/1500	27	2	1	13	8	3
SE 120/1500	10	0	0	6	3	1
IR 450/1500	19	0	3	14	2	0
Total	96	6 (6.4)	13 (13.5)	60 (62.6)	13 (13.5)	4 (4.2)

Note.—Numbers in parentheses are percentages.

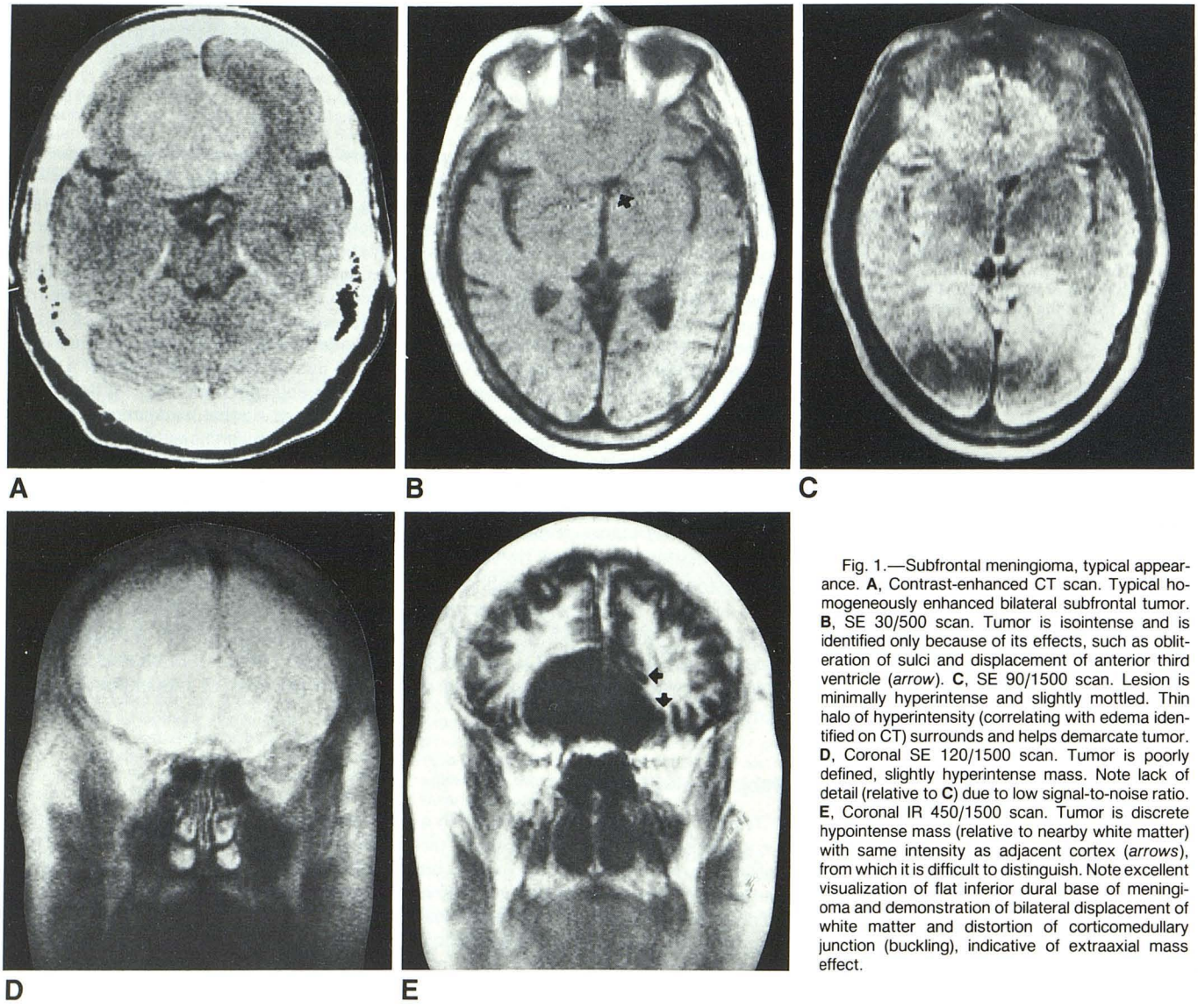

Fig. 1.—Subfrontal meningioma, typical appearance. **A**, Contrast-enhanced CT scan. Typical homogeneously enhanced bilateral subfrontal tumor. **B**, SE 30/500 scan. Tumor is isointense and is identified only because of its effects, such as obliteration of sulci and displacement of anterior third ventricle (*arrow*). **C**, SE 90/1500 scan. Lesion is minimally hyperintense and slightly mottled. Thin halo of hyperintensity (correlating with edema identified on CT) surrounds and helps demarcate tumor. **D**, Coronal SE 120/1500 scan. Tumor is poorly defined, slightly hyperintense mass. Note lack of detail (relative to **C**) due to low signal-to-noise ratio. **E**, Coronal IR 450/1500 scan. Tumor is discrete hypointense mass (relative to nearby white matter) with same intensity as adjacent cortex (*arrows*), from which it is difficult to distinguish. Note excellent visualization of flat inferior dural base of meningioma and demonstration of bilateral displacement of white matter and distortion of corticomedullary junction (buckling), indicative of extraaxial mass effect.

Results

Contrast-enhanced CT showed the lesion more clearly than MRI for 17 meningiomas (53%). In no case was MRI superior to CT in lesion detection, characterization, or delineation of tumor extent. In 15 lesions (47%), MRI and CT were of about equivalent sensitivity. Three lesions were not identified on MRI despite prior knowledge of lesion location from CT. All missed tumors were small, and none were deemed clinically significant.

The low sensitivity of MRI in the diagnosis of meningioma was the result of lack of contrast between the tumor and

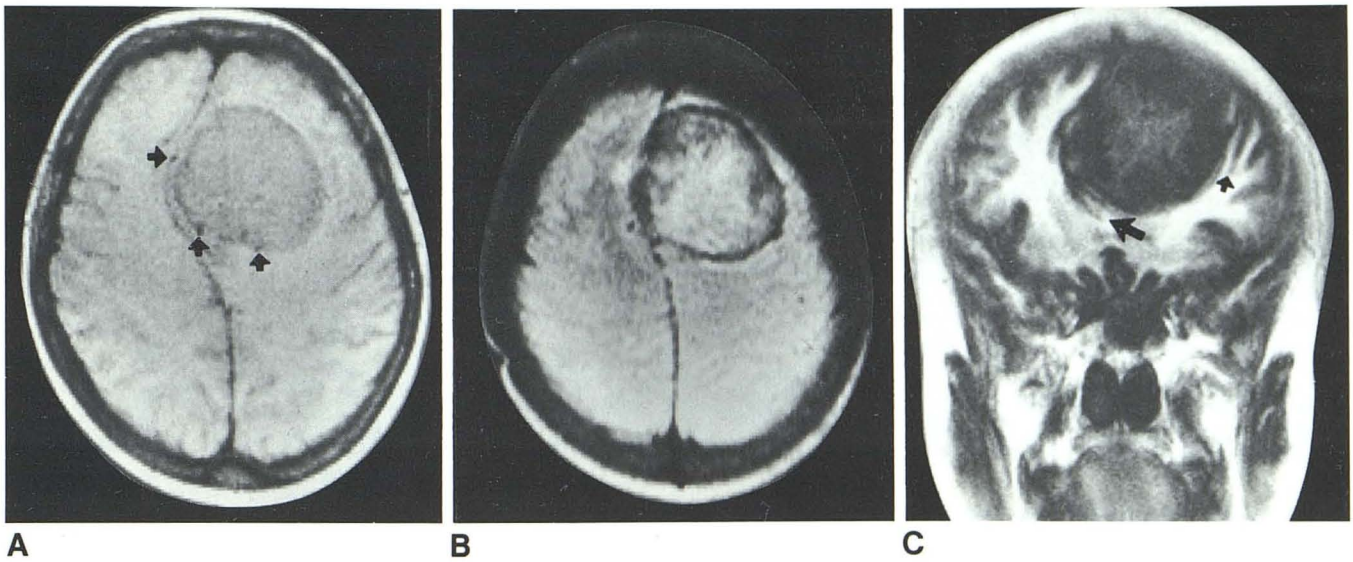

Fig. 2.—High convexity meningioma, typical features. CT scan (not shown) demonstrated densely calcified, enhancing high convexity or parasagittal meningioma. **A**, SE 30/500 scan. Slightly hypointense discrete mass. Note hypointense rim at periphery of mass. Several nodular foci of hypointensity (*arrows*) within rim. **B**, SE 90/1500 scan. Lesion has become minimally hyperintense and shows inhomogeneity and mottling. It is well demarcated from surrounding brain by discrete nodular hypointense rim and peripheral hyperintense edema collar. **C**, Coronal IR 450/1500 scan. Meningioma is seen as inhomogeneous hypointense (relative to nearby white matter) mass. Adjacent medial (*large arrow*) and lateral (*small arrow*) cortical gyri are displaced. Dural base of mass on high convexity and white matter buckling are better demonstrated on MRI than on CT.

Fig. 3.—Convexity meningioma, high contrast. **A**, SE 30/500 scan. Discrete, markedly hypointense mass with dural base on convexity. **B**, SE 120/1500 scan. Lesion is discrete, hyperintense mass. This pattern of hypointensity on T1-weighted images and hyperintensity on T2-weighted images is uncommonly seen (<10%) in meningiomas.

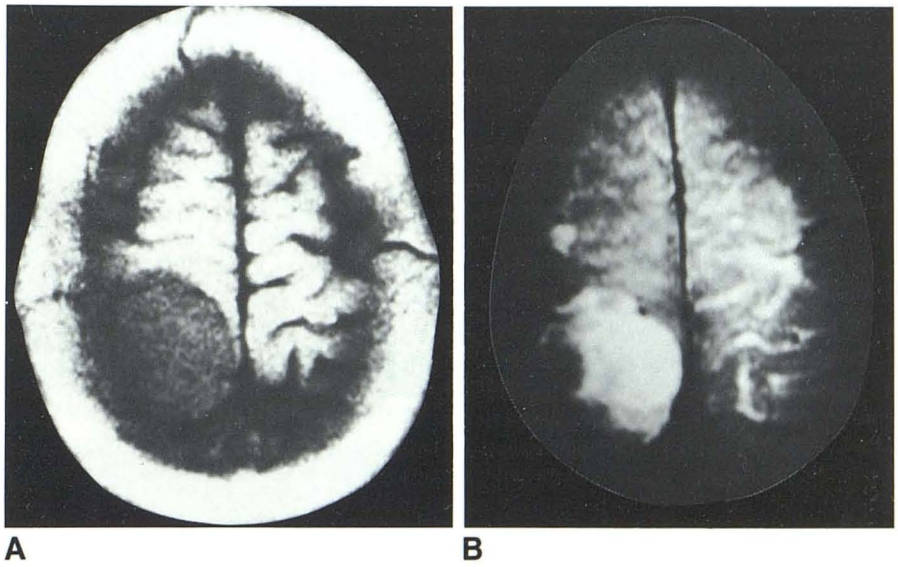

adjacent cortex (table 1), which was observed with virtually all sequences used (figs. 1 and 2). Increasing the number of sequences did not improve the sensitivity. The tumors were either isointense with adjacent cortex (figs. 1B and 1C) or showed minimal hypo- (13.5%) (fig. 2A) or hyperintensity (13.5%) (figs. 1D and 2B). Obvious hypo- (6.5%) (fig. 3A) or hyperintensity (4.2%) (fig. 3B) was encountered much less often. Although contrast was low on all sequences, altering TE or TR did affect the relative intensity of the tumor. On short TE (30 msec)–short TR (500 msec) scans, the meningiomas were hypointense (figs. 2A and 3A) or isointense (64%) (fig. 1B). In six cases, the TE was kept at 30 msec while the TR was varied. With a short TR (150–300 msec), there was no change in intensity of the tumor relative to the adjacent brain. When the TR was prolonged to 1500 msec (two cases), the tumor became relatively more intense. In one case, it remained hypointense to the adjacent cortex; in the other, it became isointense with cortex. When the TE was increased, the relative intensity of the tumor also increased. With a 60/1000 msec (TE/TR) scan, the lesions were isoin-

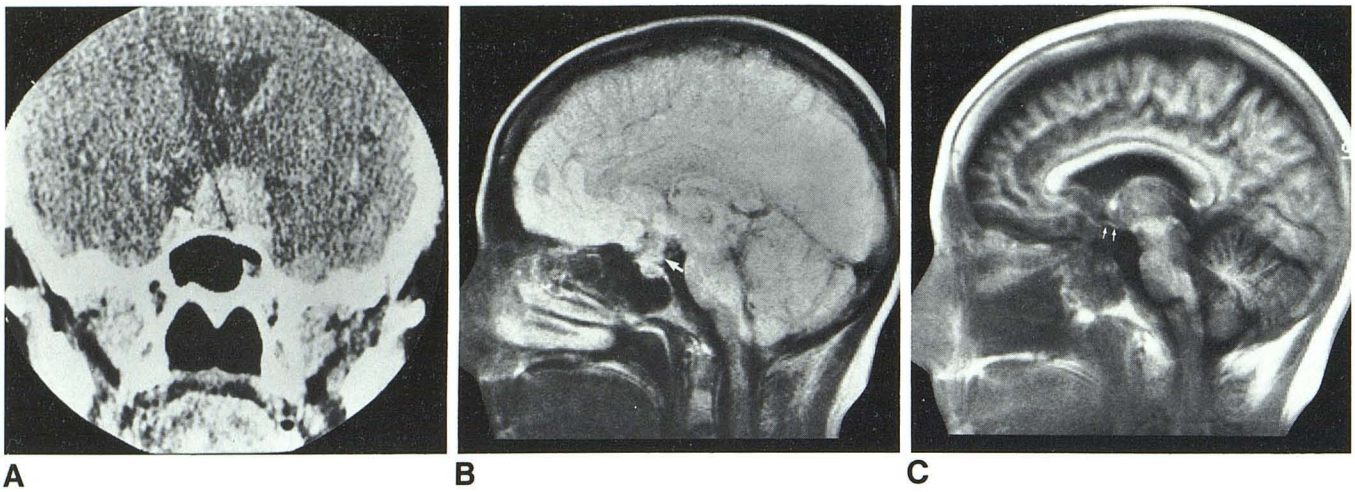

Fig. 4.—Suprasellar meningioma, typical small basal tumor. **A**, Coronal contrast-enhanced CT scan. Typical suprasellar meningioma. **B**, Sagittal SE 90/1500 scan. Poorly defined suprasellar lesion (*arrow*), which is hyperintense to CSF but isointense with both pituitary gland inferiorly and hypothalamus superiorly. **C**, Sagittal IR scan. Lesion is also poorly seen because it is isointense with adjacent CSF. Note elevation of optic chiasm (*arrows*) that allows for unequivocal diagnosis of suprasellar mass.

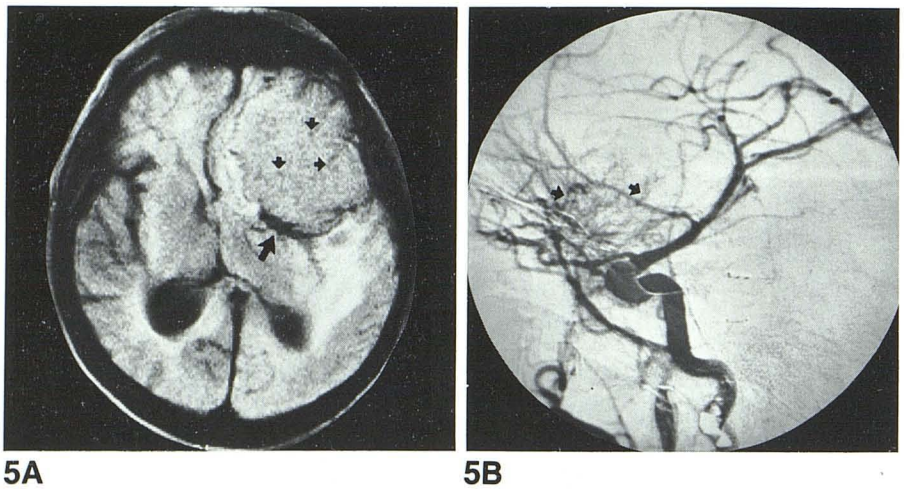

Fig. 5.—Sphenoid wing meningioma, hypointense rim and mottling. **A**, SE 90/1500 scan. Isointense mass with nodular black rim (*large arrow*), which is most prominent posteriorly. Note nodular and contiguous curvilinear foci (*small arrows*) of hypointensity within mass, which produces overall mottling effect. Signal intensity and configuration of these hypointense foci suggest that they are intratumoral vessels. **B**, Lateral common carotid angiogram confirms presence of large tumor vessels (*arrows*) in this hypervascular meningioma. **C**, Lateral angiogram, venous phase. Tumor blush and prominent venous capsule posteriorly and superiorly (*arrows*) correlating well with black rim on MRI.

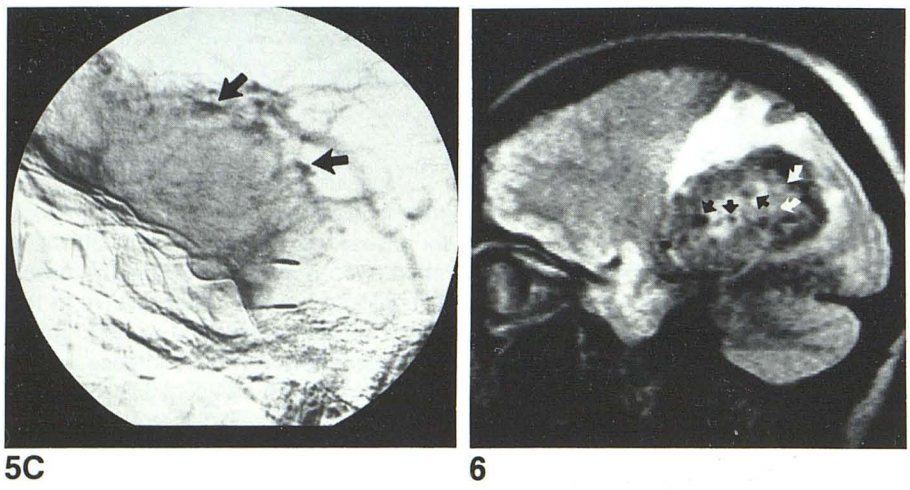

Fig. 6.—Falx tentorial meningioma, mottling and edema. Sagittal SE 90/1500 scan. Marked tumor mottling with large dark foci (*black arrows*) and several bright foci (*white arrows*). Angiogram (not shown) demonstrated extensive hypervascularity with large intratumoral vessels and rapid arterial venous shunting. Note edema collar, which helps demarcate tumor from adjacent brain. CT (not shown) demonstrated densely calcified meningioma.

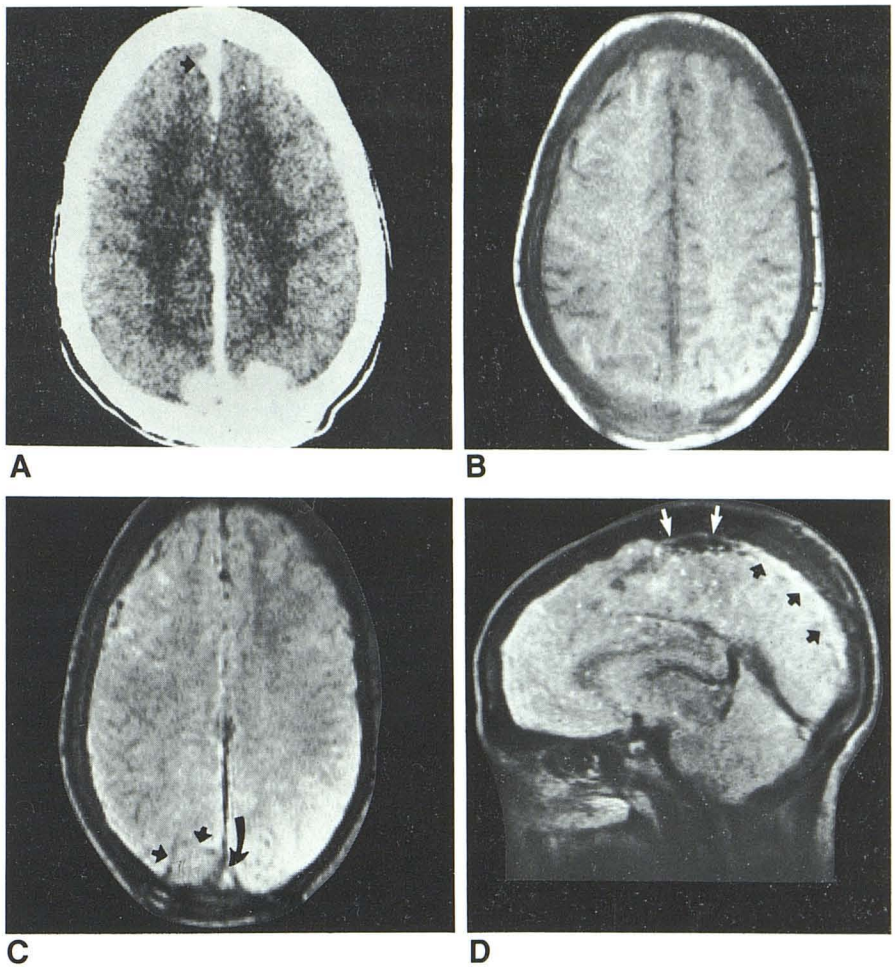

Fig. 7.—Multiple parasagittal meningiomas, hyperostosis and vascular effects. **A**, Contrast-enhanced CT scan. Small bilateral posterior parasagittal/convexity meningiomas. Small parafalcial meningioma is noted anteriorly (*arrow*). Bone thickening is suspected, but hyperostosis was well seen only when bone window settings were used. **B**, SE 30/500 scan. Tumors are very difficult to see because they are isointense with adjacent brain. Indirect signs of mass effect include absence of sulci and obliteration of posterior interhemispheric fissure and falx. Note increased thickness of calvaria and loss of definition of inner and outer table due to diffuse increase in intensity of involved bone. (Lateral to lesion on left, normal hypointense inner and outer tables [cortical bone] are seen around more intense diploic space.) **C**, SE 90/1500 scan. Lesions remain isointense. Right lesion is demarcated by black rim (*small arrows*). More anterior lesion is not visualized. Bone changes are less well seen than on **B**. Note increased signal in superior sagittal sinus (*large arrow*) due to slow flow. **D**, Sagittal SE 90/1500 scan. Diffuse increased signal in posterior aspect of superior sagittal sinus (*black arrows*). Anteriorly, prominent hypointense foci (*white arrows*) represent collateral venous channels around involved superior sagittal sinus (confirmed in angiography). Tumor invasion of superior sagittal sinus was surgically confirmed.

tense with cortex in seven of eight cases. When the TE was prolonged to 90 msec and the TR to 1500 msec, the lesions were isointense with (48%) (figs. 1C, 4B, 5A, 6, and 7B) or hyperintense to (41%) (figs. 2B, 8B, and 9) the adjacent cortex. Two small, densely calcified meningiomas remained hypointense on 90/1500 msec (TE/TR) scans. Prolongation of the TE to 120 msec did not increase the contrast between the tumor and the adjacent brain (fig. 1D) (table 1), and the 90-msec-TR scans were of superior quality due to a better signal-to-noise ratio (cf. figs. 1C and 1D). Five studies were done with longer TRs (2000–2500 msec), and there was no significant change in contrast when compared with 1500-msec-TR scans.

Because of the lack of intrinsic contrast, tumor identification was dependent on demonstration of anatomic distortion. Those imaging sequences that provided the greatest anatomic detail were, therefore, the most diagnostically informative. SE scans with short TE (30 msec) and long TR (1500 msec) were valuable, as they showed excellent anatomic detail such as the interface between gray and white matter. Displacement or "buckling" of white matter (a highly characteristic CT feature of extraaxial masses [11]), was nicely demonstrated with this technique but was best seen on IR scans (figs. 1E, 2C, and 4C). This pulse sequence produces maximal gray/white matter differentiation [2, 12, 13], thus providing the best anatomic detail for differentiating intra- from extraaxial masses. On IR, the meningiomas were nearly isointense with adjacent cortex (figs. 1E and 2C) and/or cerebrospinal fluid (CSF) (fig. 4C) and were markedly hypointense to nearby white matter. Therefore, on IR, the large tumors appear as dark, discrete masses displacing brain substance (figs. 1E and 2C). With small lesions, the excellent gray/white differentiation allowed for identification of subtle extraaxial mass effect (buckling) and more definitive tumor detection than was possible with SE technique (fig. 4B).

Several MRI features were helpful in delineating the tumor from the adjacent brain and specifically characterizing it as a meningioma (table 2). A hypointense rim was identified at the tumor periphery on multiple pulse sequences in 19 out of 32 lesions (figs. 2, 3, 5, and 6). The absence of signal from the rim on multiple sequences suggested a vascular origin, which was confirmed at angiography where a prominent venous capsule and/or displaced major artery (anterior or middle cerebral artery branch) was seen at the margin of the tumor (fig. 5). Nodular foci of hypointensity within or adjacent to the dark rim was a characteristic feature representing vessels

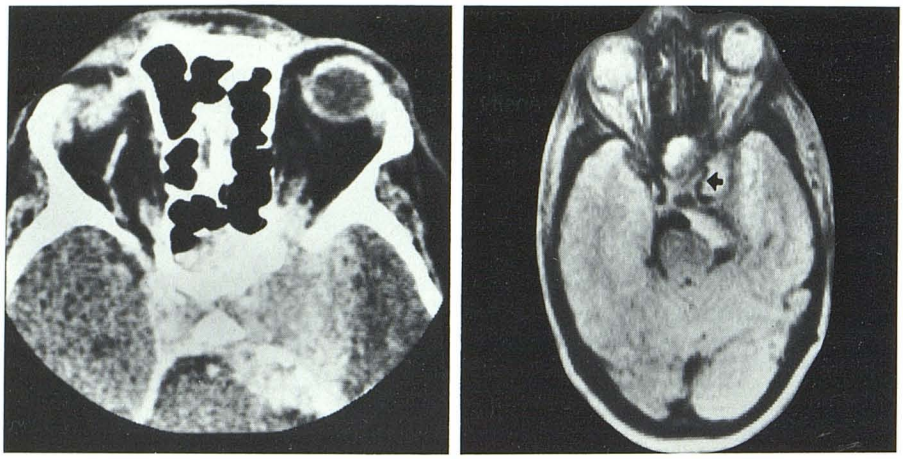

A B

Fig. 8.—Left parasellar meningioma, arterial encasement. **A**, Contrast-enhanced CT scan. Parasellar meningioma. Enhanced (dense) carotid artery cannot be seen within enhanced (dense) tumor. **B**, SE 90/1500 scan. Tumor is poorly defined, mildly hyperintense lesion. Within tumor, hypointense carotid artery is easily identified. Its proximal part is narrower (*arrow*) in caliber than contralateral carotid artery. Angiography confirmed encasement and narrowing of this vessel. Proximal left posterior cerebral artery is not visualized because of displacement (confirmed on other scans).

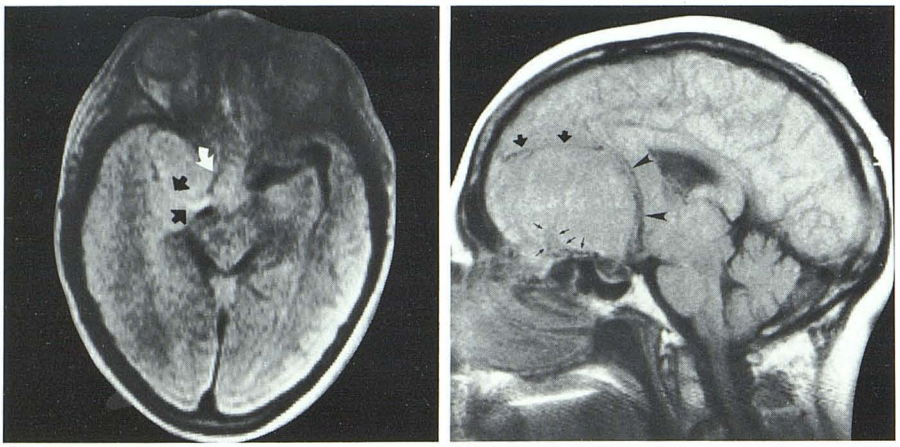

9 10

Fig. 9.—Sphenoid wing meningioma, arterial encasement and diminished flow. SE 90/1500 scan. Poorly defined, mildly hyperintense medial sphenoid and suprasellar lesion. Right internal carotid artery is encased and medially displaced (*white arrow*). Middle cerebral artery is posteriorly displaced, and its proximal segment has increased signal (*black arrows*). Angiography revealed marked diminution of flow in middle cerebral artery.

Fig. 10.—Subfrontal meningioma, arterial displacement and vascular pedicle. Sagittal SE 30/500 scan. Isointense tumor identified because of bulk posterior displacement of corpus callosum. Note posterior superior displacement without encasement of pericallosal artery (*arrowheads*) and superior displacement of frontal polar or gyrus rectus branch (*large arrows*). Dilated ethmoidal perforating branches of ophthalmic artery and vascular pedicle of tumor are well demonstrated (*small arrows*).

seen in cross section (figs. 2A, 2B, 5A, and 7C). We have not encountered this finding in over 40 supratentorial gliomas but have identified a smooth black rim in two metastatic foci on long TE–long TR (90/1500) scans only. We have also identified a smooth black rim adjacent to two other extraaxial tumors, a fifth-nerve neurinoma and a metastatic focus.

A second characteristic feature was the inhomogeneity or mottling of the tumor especially on long TE–long TR scans (90/1500). The mottling ranged from fine stippling (figs. 1C, 2B, and 5A) to more coarse and irregular nodularity (fig. 6). Mottling correlated best with angiographic and surgical evidence of tumor hypervascularity, suggesting that the nodules represented intratumoral vascular channels, with varying flow rates accounting for the variable intensity of the nodules (figs. 5 and 6) [14, 15]. The nodularity did not correlate with other features, such as calcification or irregular enhancement on CT. It was not seen in intraaxial lesions, such as gliomas or metastases.

The presence and extent of edema was better visualized with MRI (SE 90/1500) than with CT. In addition, the edema did not obscure the underlying tumor as it often does with parenchymal masses (figs. 1C, 2B, and 6) [3, 5, 7]. The tumor was less intense than the adjacent edema, so the edema collar helped demarcate the tumor from the adjacent brain.

Bone changes were demonstrated on MRI in 11 of 16 patients with CT evidence of bony abnormalities. In one case, bony involvement was demonstrated on MRI alone. Hyperostosis produced obvious bone thickening (fig. 7B), and the normal landmarks of the calvaria were obliterated. Normally the inner and outer tables of the skull were seen as linear hypointensities (cortical bone) sandwiched around the more intense diploic space. In meningiomas, the bone involvement produced increased intensity of the cortex, which blended with the diploic space to produce an amorphous appearance of the affected bone (figs. 7B and 7C). An advantage of MRI is that these findings were seen on the routine images used to identify brain anatomy and pathology, whereas on CT special bone window settings had to be obtained to demonstrate the presence and degree of osseous involvement.

Aside from the lack of tumor contrast, the major limitation

TABLE 2: **MRI Findings in Meningioma**

	MRI Positive	MRI positive/CT positive	MRI negative/CT positive	MRI positive/CT negative
Black rim ($n = 32$)	19	...	...	...
Mottling ($n = 32$)	14	...	...	...
Calcification ($n = 15$)	3	...	...	...
Bone involvement	...	11	5	1
Edema	...	15	0	7

of MRI was the inability to identify tumor calcifications. Three small, densely calcified meningiomas showed hypointensity on SE 90/1500 scans presumably because of an absence of signal from the calcified tumor. In the remaining 12 cases, including several largely densely calcified meningiomas, the calcification was invisible on MRI (figs. 2 and 6).

MRI was superior to CT in the visualization of vascular effects of the tumor. On MRI the absence of signal from flowing blood [14, 15] causes the vessels to appear black within the brighter tumor (fig. 8B). On contrast-enhanced CT, on the other hand, both the vessels and tumor are dense and, therefore, indistinguishable (fig. 8A). Improved visualization of vascular anatomy was particularly helpful in evaluating the large number of basal tumors in this series (figs. 8 and 9). Arterial narrowing due to encasement (e.g., of the cavernous carotid artery) was identified and differentiated from simple displacement (fig. 10). In fact, MRI provided angiographic "roadmap" information equivalent to that obtained by digital intravenous angiography and often eliminated the need for this procedure. Increasing intravascular signal due to diminution of flow (paradoxic effect) [14, 15] was observed in three cases. In one patient, a sphenoid wing meningioma produced encasement and narrowing of the carotid and middle cerebral arteries (fig. 9); in two patients, increased signal within the superior sagittal sinus because of tumor invasion and diminished flow was identified and confirmed both angiographically and at surgery (fig. 7). The multiplanar capacities of MRI allowed for excellent visualization of collateral venous drainage around the involved superior sagittal sinus (fig. 7D). Finally, the vascular pedicle of the tumor and the major feeding extracerebral arteries were identified in two patients (fig. 10).

Discussion

Meningiomas are the most common benign intracranial neoplasms [9, 10]. Therefore, identification of these treatable tumors by an imaging method used (or proposed for use) [7] as a screening procedure is of paramount importance. CT is both sensitive and specific in the diagnosis of meningioma [16–18]. Sensitivity arises from the high contrast between the tumor and the adjacent brain on contrast-enhanced scans [18]. MRI is less sensitive than CT in the diagnosis of meningioma because there is a lack of contrast between the tumor and the adjacent cortex (table 1). This is unusual, because most other intracranial tumors show better intrinsic contrast on MRI than on CT because of prolongation of both T1 and T2 [2, 5–7]. These changes in relaxation times are manifested as hypointensity on T1-weighted images (short TE–short TR) and marked hyperintensity on T2-weighted images (long TE–long TR). Meningiomas have the same general pattern of relative intensity but to a much smaller degree. On T1-weighted images (30 msec TE, 150–500 msec TR), the tumors were hypointense in 37.5% of cases (figs. 2A and 3A) and isointense in 62.5% of cases (figs. 1B, 7B, and 10). Scans with intermediate TE and TR (e.g. 60/1000) showed a combination of T1 and T2 effects that tended to cancel each other out, producing lesions that were isointense [7]. On T2-weighted images (90–120 msec TE, 1500–2500 msec TR), tumors were isointense in 51% (figs. 1C, 4B, 5A, 6, and 7B) and hyperintense in 40% of cases (figs. 2B, 8B, and 9). The lack of contrast on multiple scan sequences would suggest that factors that affect intensity, such as proton density, T1, and T2, are similar in meningiomas and cortical brain. This has been confirmed using in vivo [2, 12] and in vitro [19, 20] measurements of meningioma tissue. Marked hypo- or hyperintensity was encountered in 10% of images, and those tumors with high contrast had it both on T1- (hypointense) and T2- (hyperintense) weighted images, suggesting that these lesions may have a higher water content than the typical meningioma [7, 21] (fig. 3). If this finding is pathologically confirmed, it might aid in preoperative planning by allowing for prospective identification of those tumors that are softer (more fluid).

Improved contrast would increase sensitivity, and this might be obtained by several techniques. First, prolonging the TE should allow for detection of subtle T2 differences between the tumor and the adjacent cortex. In our series, prolonging the TE from 90 to 120 msec, however, did not achieve increased sensitivity (table 1). The 120-msec-TE images were of poor quality due to low signal-to-noise ratio (cf. figs. 1C and 1D). Improvement in the signal-to-noise ratio can be achieved by increasing magnetic strength [6, 22], and it remains to be seen if meningiomas will be better demonstrated on imagers that use high-field-strength magnets (1–2 T) and long TE (greater than 100 msec). A more certain method of improving contrast is the use of paramagnetic contrast agents. Gadolinium-DPTA, for example, produces enhancement analogous to that seen with iodinated contrast agents [21, 23]. Since meningiomas show excellent enhancement on CT [16–18], it is expected that they will enhance on MRI as well. (Several instances of dramatic enhancement of meningiomas on MRI with gadolinium-DPTA have recently been presented [21].) The desirability of performing contrast-enhanced MRI for identification of this common lesion, however, may have significant implications in defining the "routine" or "screening" protocols for MR scanning.

Although the lack of contrast makes meningiomas less obvious than other lesions on MRI, most tumors may be identified because of their effects (displacement and edema) on adjacent brain. Diagnostic difficulties arise when the meningiomas are small and have minimal mass effect and little or no edema, as is typical of basal lesions [18] (figs. 4 and 8). In these cases, careful attention is required to identify the subtle anatomic distortion that is the key to correct diagnosis. Those pulse sequences that produce the sharpest anatomic

detail are of greatest diagnostic value. Thus, SE sequences with a short TE (e.g., 30 msec) and long TR (1500–2500 msec) and in particular IR scans are most informative because of their superior gray/white matter differentiation [2, 12, 13]. Displacement of the white matter away from the mass and distortion and flattening of the corticomedullary junction (buckling) typical of extraaxial masses [11] is dramatically demonstrated with this technique (figs. 1E and 2C) and was especially helpful in demonstrating several small parasellar lesions (fig. 4). Although the meningiomas are isointense with adjacent cortex and/or spinal fluid on IR scans, they are seen as a discrete dark mass in marked contrast to nearby white matter. Using the multiplanar capacity of MRI, the dural base of the mass may be better demonstrated than on CT (figs. 1E and 2C).

Identification of a dural base and white matter displacement and buckling allow for a specific diagnosis of meningioma on MRI (as they do on CT) [17], something that is often not possible with other lesions on MRI [2, 3, 5–8, 12]. Other characteristic MRI features aid in specific diagnosis of meningioma and are analogous to specific CT features [16–18]. First, the lack of contrast, which so limits sensitivity, ironically increased specificity since most masses show greater hyperintensity on T2-weighted images [3, 5–8, 12, 21]. Two characteristic features, the peripheral black rim and mottling, appear to be related to vascular effects. The hypointense rim was seen in two-thirds of our cases (figs. 2, 3, 5, and 6). Since it is present on multiple sequences (as opposed to the black rim occasionally encountered only on T2-weighted images in cerebral metastases), the hypointensity of the rim is most likely a flow effect within the venous capsule (fig. 5) and/or occasionally in larger adjacent arteries [14, 15]. The mottling is most apparent on T2-weighted images, and it correlated well with angiographically demonstrable tumor hypervascularity (figs. 5 and 6). The mottling was caused by the presence of nodular and in some instances (fig. 5A) curvilinear foci of both hypo- and hyperintensity that were highly suggestive of small vessels seen tangentially and in cross section. The variation in intensity of these nodules may reflect variable rates of flow in intratumoral vessels. Other possible causes of mottling, such as tissue inhomogeneity or calcification, could not be documented by correlation with CT or pathologic findings. This phenomenon has not been seen in hypervascular intraaxial lesions, such as gliomas, possibly because the hypervascular gliomas studied so far have been necrotic and, thus, homogeneously hyperintense due to increased fluidity. The uncommon combination of a hypervascular solid intraaxial tumor might show nodularity.

Two classic pathologic findings of meningiomas, calcification and hyperostosis [9, 10], were demonstrated with drastically different degrees of success. Calcification was poorly detected. It was not seen in 12 of 15 tumors with obvious calcification on CT (figs. 2 and 6). Three small, densely calcified lesions were hypointense on T2-weighted images, possibly reflecting the solidity of these tumors. In most of the tumors, however, the calcifications were invisible. Presumably, in these cases the chemical state of the calcium did not alter the environment of nearby hydrogen ions and, therefore, did not affect intensity [3, 7]. Hyperostosis was demonstrated with much greater success (fig. 7), even though cortical bone has no signal and previous authors have expressed reservations about the ability of MRI to demonstrate bone changes [2]. Increased thickness of the calvaria was easily detected, and the involved cortex showed a moderate increase in signal. The contrast normally present between the hypointense inner and outer tables and the hyperintense diploic space was lost when the cortical bone became hyperintense, producing an amorphous appearance to the involved bone (fig. 7b). Of the five cases of CT-confirmed hyperostosis of the sphenoid bone missed on MRI, four might have been detected had scans in the coronal plane (perpendicular to the area of hyperostosis) been obtained. In general, bone changes were best seen on T1-weighted images (cf. figs. 7B and 7C), and MRI has the advantage over CT in demonstrating bone changes on routine images (cf. figs. 7A and 7B). On CT, special window width and level adjustments are necessary to demonstrate the extent of the bone involvement.

Finally, vascular effects were much better demonstrated on MRI than on CT. Arterial encasement in particular at the base of the brain is well seen on MRI because of the low signal seen in areas of rapid blood flow [14, 15]. Encasement and narrowing of the carotid artery was seen in several parasellar meningiomas (figs. 8B and 9) using multiplanar scanning. Displacement without encasement could also be easily identified (fig. 10). Identification of the vascular pedicle of the meningioma and its extracerebral blood supply was also occasionally encountered (fig. 10). Increased signal within a vessel is indicative of slower flow (paradoxic effect) [14, 15], and the identification of this phenomenon in a middle cerebral artery encased by a sphenoid wing meningioma (fig. 9) correlated well with angiographic evidence of marked diminution of flow. In two patients with parasagittal meningiomas, increased signal in the superior sagittal sinus adjacent to the lesion was indicative of angiographically and surgically confirmed tumor invasion (figs. 7C and 7D). Although the angiographic detail on MRI does not equal that of selective angiography, it does provide information equal or superior to that obtained with digital intravenous angiography; thus, in those patients undergoing MRI, digital venous angiography may often be eliminated. When MRI demonstrates involvement of a venous sinus, digital venous angiography or arteriography may be performed to differentiate partial from complete sinus occlusion.

REFERENCES

1. Young IR, Hall AS, Pallis CA, Legg NJ, Bydder GM, Steiner RE. Nuclear magnetic resonance imaging of the brain in multiple sclerosis. *Lancet* **1981**;2:1063–1066
2. Bydder GM, Steiner RE, Young IR, et al. Clinical NMR imaging of the brain: 140 cases. *AJNR* **1982**;3:459–480, *AJR* **1982**;139:215–236
3. Brant-Zawadzki M, Davis PL, Crooks LE, et al. NMR demonstration of cerebral abnormalities: comparison with CT. *AJNR* **1983**;4:117–124, *AJR* **1983**;140:847–854
4. Lukes SA, Crooks LE, Aminoff MJ, et al. Nuclear magnetic

resonance imaging in multiple sclerosis. *Ann Neurol* **1983**;6:592–601
5. Brant-Zawadzki M, Badami JP, Mills CM, Norman B, Newton TH. Primary intracranial tumor imaging: comparison of magnetic resonance imaging and CT. *Radiology* **1984**;150:435–440
6. Weinstein MA, Modic MP, Pavlicek W, Keyser CK. Nuclear magnetic resonance for the examination of brain tumors. *Semin Roentgenol* **1984**;19:139–147
7. Brant-Zawadzki M, Norman D, Newton TH, et al. Magnetic resonance imaging of the brain: the optimal screening technique. *Radiology* **1984**;152:171–177
8. Zimmerman RA, Bilaniuk LT, Goldberg HI, et al. Cerebral NMR imaging: early results with a 0.12 T resistive system. *AJNR* **1984**;5:1–7, *AJR* **1983**;141:1187–1193
9. Zülch KJ. *Atlas of gross neurosurgical pathology*. New York: Springer-Verlag, **1975**:113–135
10. Wilson CB, Moossy J, Boldery E, Malamud N. Pathology of intracranial tumors. In: Newton TH, Potts DG, eds. *Radiology of the skull and brain*, vol 3, *Anatomy and pathology*. St. Louis: Mosby, **1977**:3016–3049
11. George AJ, Russell EJ, Kricheff II. White matter buckling: CT sign of extraaxial intracranial mass. *AJNR* **1980**;1:425–450, *AJR* **1980**;135:1031–1036
12. Mills CM, Crooks LE, Kaufman L, Brant-Zawadzki M. Cerebral abnormalities: use of calculated T1 and T2 magnetic resonance images for diagnosis. *Radiology* **1984**;150:87–94
13. Doyle FH, Gore JC, Pennock JM, et al. Imaging of the brain by nuclear magnetic resonance. *Lancet* **1981**;2:53–57
14. Crooks LE, Mills CM, Davis PL, et al. Visualization of cerebral and vascular abnormalities by NMR imaging: the effects of imaging parameters on contrast. *Radiology* **1982**;144:843–852
15. Mills CM, Brant-Zawadzki M, Crooks LE, et al. Nuclear magnetic resonance: principles of blood flow imaging. *AJNR* **1983**;4:1161–1166, *AJR* **1984**;142:165–170
16. New TJ, Aronov S, Hesselink J. National Cancer Institute study: evaluation of computed tomography in the diagnosis of intracranial neoplasm. IV. Meningiomas. *Radiology* **1980**;136:665–675
17. Russell EJ, Kricheff II, Budzilovich GN, et al. Atypical computed tomographic features of intracranial meningiomas: radiological-pathological correlation in a series of 130 consecutive cases. *Radiology* **1980**;135:673–682
18. Rosenbaum AE, Rosenbloom SD. Meningiomas revisited. *Semin Roentgenol* **1984**;19:8–26
19. Araki T, Inouye T, Suzuki H, Machida T, Lio M. Magnetic resonance imaging of brain tumors: measurement of T1. Work in progress. *Radiology* **1984**;150:95–98
20. Rinck P, Meindel S, Bieler U, et al. Tumor grading and discrimination by CPMG sequences and in vitro T2 measurements. Presented at the annual meeting of the Society of Magnetic Resonance in Medicine, New York, August **1984**
21. Bydder GM. Magnetic resonance imaging of tumors of the central nervous system. Presented at the annual meeting of the Society of Magnetic Resonance in Medicine, New York, August **1984**
22. Hart HR, Bottomley PA, Edelstein WA, et al. Nuclear magnetic resonance imaging: contrast-to-noise ratio as a function of strength of magnetic field. *AJR* **1983**;141:1195–1201
23. Grossman RI, Wolf G, Biery D, et al. Gadolinium enhanced nuclear magnetic resonance images of experimental brain abscess. *J Comput Assist Tomogr* **1984**;8:204–207